LETTER

Lithium Iron Phosphate Superbattery for Mass-Market Electric Vehicles

Jie Liao, Ryan S. Longchamps, Brian D. McCarthy, Feifei Shi,* and Chao-Yang Wang*

Read Online

ACCESS | 📊 Metrics & More | 📖 Article Recommendations | 🆘 Supporting Information

ABSTRACT: Narrow operating temperature range and low charge rates are two obstacles limiting $LiFePO_4$-based batteries as superb batteries for mass-market electric vehicles. Here, we experimentally demonstrate that a 168.4 Wh/kg $LiFePO_4$/graphite cell can operate in a broad temperature range through self-heating cell design and using electrolytes containing LiFSI. Remarkable high-temperature stability with 6100 h of cycle life was achieved at 60 °C. With self-heating, the cell can deliver an energy and power density of 90.2 Wh/kg and 1227 W/kg, respectively, even at an ultralow temperature of −50 °C, compared to almost no performance for cells without self-heating. The heating process took 164 s and only 0.161% of the cell energy per degree of temperature rise. Fast charging at a 6C rate was achieved at all ambient temperatures. The total preheating and charging time was less than 12 min, and the cell finished 2500 cycles of 6C charging while still retaining 81.3% capacity.
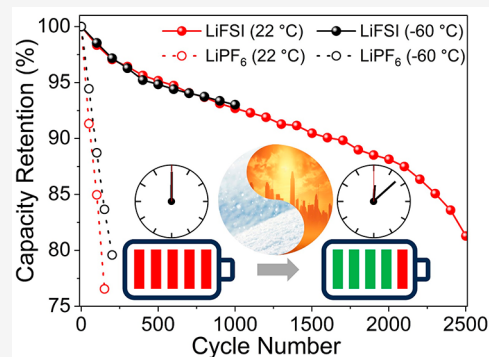
Transportation electrification has shifted from a period of luxury buyers and early adopters to a mass market. A successful shift relies on the solution to three remaining pain points: range anxiety, charging anxiety, and cost competitiveness with internal combustion engines.[1,2] In the earlier work, we have elucidated that a downsized battery pack that is 10 min rechargeable will ideally resolve the above-mentioned three challenges.[3] Here, we aim to experimentally develop such a superbattery based on lithium iron phosphate (LFP) cathodes that is thermally modulated to offer high-temperature stability up to 90 °C and hence superior safety, outstanding power and energy at ultralow temperatures down to −50 °C as well as 10 min charging to 80% state of charge (SOC) with >2500 cycles. The combination of low cost, abundance of LFP raw materials,[2,4] intrinsic safety, and extremely long life[5,6] makes a thermally modulatory LFP battery an ideal candidate for mass-market electric vehicles and hence decarbonization.

LFP baseline batteries are known to face major problems, such as low energy density (ca. 170 Wh/kg) and relatively poor rate capability due to its low electronic conductivity (in the order of 10^{-9} S/cm), which result in limited range of electric vehicles (EVs) and poor charging performance, especially at low temperatures.[6−11] The impact of high temperature on the battery is, however, more complex, which may involve accelerated reactions between the electrolyte and electrodes and undesired side reactions such as the decomposition of solvents or salts.[12] Although an LFP cathode

is relatively thermally stable, it can still be attacked by the decomposition product of the electrolyte (such as HF) at elevated temperatures, which results in Fe dissolution.[13] Extensive efforts have been made to optimize the electrolyte formulations to expand the operating temperature range of batteries.[14] The lithium bis(fluorosulfonyl)imide (LiFSI) salt is believed to be superior to lithium hexafluorophosphate (LiPF₆) and improves both low-temperature and high-temperature stability, due to its high thermal stability, moisture resistivity, and lower degree of ion-association.[15−17] Although aluminum corrosion may occur when LiFSI is used as the single salt and the cathode potential is above 4.2 V vs Li⁺/Li, this will not be a problem for LFP batteries, since its operating voltage is usually below 3.65 V.[16] As for the solvents, the quest is still ongoing in order to satisfy the need for the combination of high liquidus range, stability, cost-effectiveness, and ecofriendliness simultaneously.[12,14]

Recently, the self-heating battery (SHB) with a Ni foil embedded inside the electrode layers to heat the cell using its own energy provides a new route to tackle the low-temperature issue of batteries without having to modify solvents; thus, low
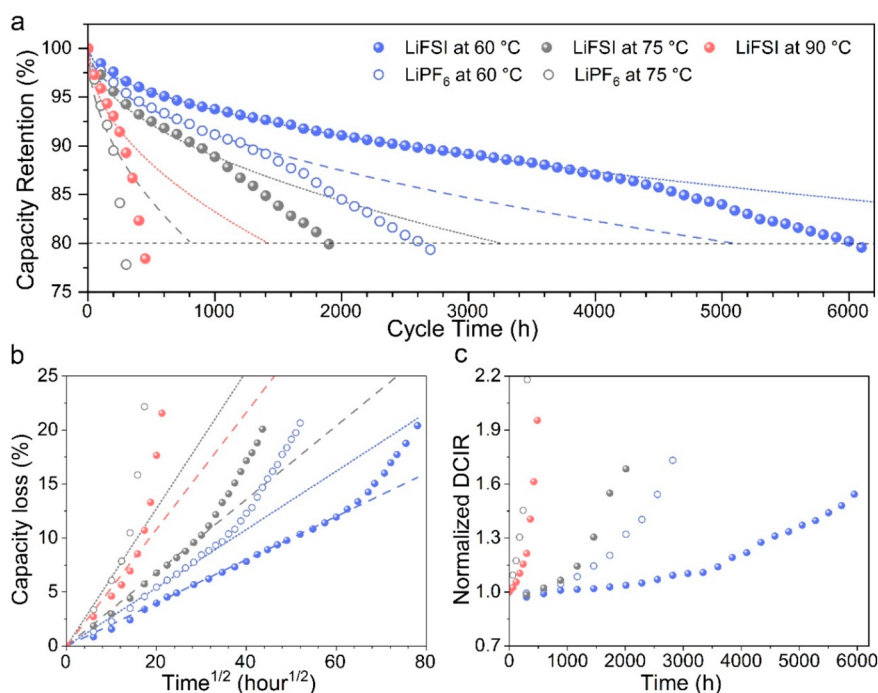
Figure 1. High-temperature cycling stability. (a) Capacity retention of the cells with respect to cycle time; (b) capacity loss against the square root of time; (c) normalized direct current internal resistance (DCIR) with cycle time.

temperature became little concern.[3,18,19] In addition to the wide temperature range for power and energy output, fast charging is also a critical aspect for the batteries, especially for LFP batteries with low energy densities because they need quick "re-fueling" to address the range anxiety.[18] LFP was believed to have low rates due to its low electronic conductivity and sluggish kinetics for lithium diffusion and insertion/deinsertion in the crystal.[6] Although these issues have been improved by nanominiaturization and carbon coating, at an ultrahigh rate of 6C, potential challenges may still persist, especially for energy-dense batteries with thick electrodes.[20,21] Another problem with fast charging is lithium plating, which not only causes rapid capacity decay but also poses safety concerns.[22] Since the transport and diffusion of Li^+ in the electrolyte and through the cathode/anode are temperature-dependent and follow the Arrhenius law, both can be greatly enhanced by raising the temperature, and thus, fast charging can be greatly facilitated at elevated temperatures.[23] The SHB has demonstrated successful extreme fast charging (XFC) for $LiNi_{1-x-y}Co_xMn_yO_2$/graphite batteries by rapidly heating the cell to 60 °C to eliminate lithium-plating.[18,24] For LFP/graphite cells, LiFSI can be used as the single salt, which is more beneficial for the high-temperature stability and fast-charging capability.[18]

In this work, we experimentally demonstrate that an 11-Ah LFP/graphite cell with a high energy density of 168.4 Wh/kg can be operated in a wide temperature range and be charged at 6C regardless of ambient temperatures through rapid internal heating. In the cells, a mixture of 30% ethylene carbonate (EC) and 70% diethyl carbonate (DEC) was used as the solvent (mass ratio), and 1.2 M LiFSI or $LiPF_6$ was used as the salt for comparison. DEC was chosen over dimethyl carbonate (DMC) and ethyl methyl carbonate (EMC) due to its wider liquidous temperature range (−74.3 to 126 °C).[25] The cells with LiFSI were named FSI and cells with $LiPF_6$ were named

PF6. The use of LiFSI salt and DEC improved the high-temperature stability, and FSI exhibited superior cycling stability at high temperatures and could be cycled even at 90 °C, at which PF6 failed. With self-heating, FSI was able to provide an energy density of 90.2 Wh/kg and power density of 1227 W/kg even at an ultralow temperature of −50 °C, compared to 51.8 Wh/kg and 993 W/kg for PF6, or almost no performance at all for cells without self-heating. The self-heating of FSI is generally quicker and slightly more efficient than PF6. It took 164 s and 10.40% of the cell energy of FSI to heat from −50 to 10 °C, compared to 190 s and 11.07% for PF6. As for fast charging, both cells were able to achieve 6C fast charging through rapid internal preheating, regardless of ambient temperatures. However, PF6 suffered from fast capacity fade, with 80% of capacity retention reached in less than 200 cycles, while FSI finished 2500 cycles of 6C charging and still has a capacity retention of 81.3%. The present study promises an LFP-based superbattery for mass-market EVs.

Remarkable high-temperature stability. High-temperature stability is crucial for batteries, especially in hot summers, with surging air temperatures. Although olivine-structured LFP is considered more thermally and chemically stable than the layer-structured $LiNi_{1-x-y}Co_xMn_yO_2$, it can be attacked by HF generated by $LiPF_6$ with a trace amount of water and suffer from Fe dissolution, especially at high temperatures.[13,16,26] The use of LiFSI with superior tolerance to heat and moisture can effectively improve the cycle stability at high temperatures. Figure 1 shows the cycle stability of the cells at different temperatures. The cells were charged and discharged at a C/3 rate, with a 10 min rest step between each charging and discharging step. As shown in Figure 1a, the cycle life of a cell decreases with increasing ambient temperature, and FSI generally had better capacity retention than PF6. At 60 °C, FSI could be cycled for 6100 h (991 cycles) before reaching a capacity loss of 20%, while PF6 survived only 2800 h (462
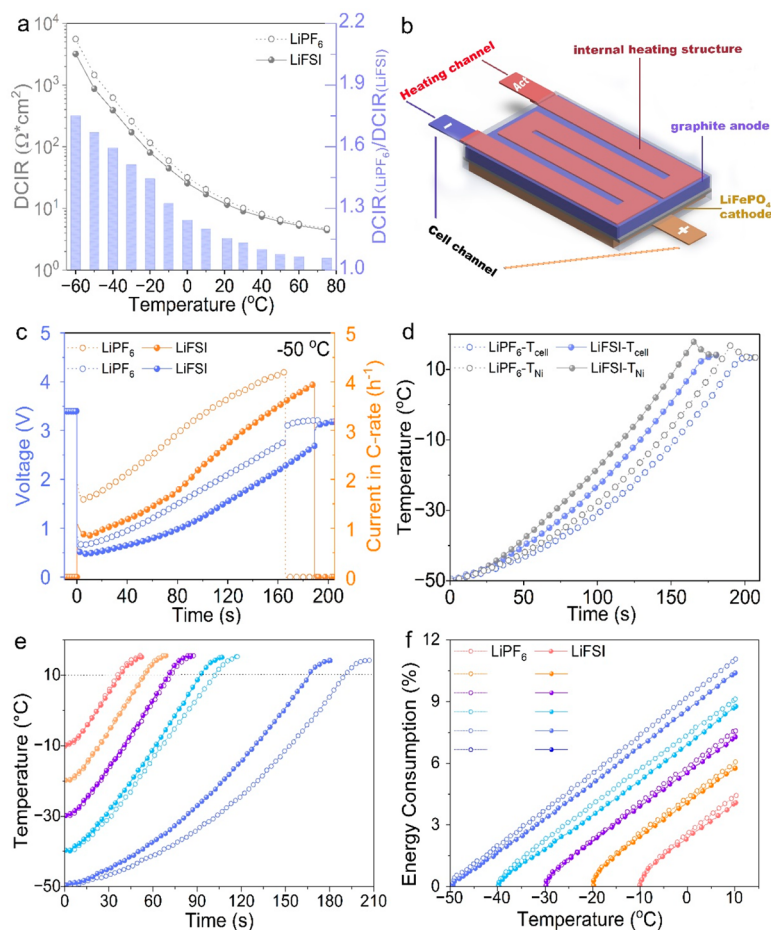
Figure 2. Self-heating LFP batteries: (a) The direct current internal resistance (DCIR) of the cells at different temperatures; (b) schematic configuration of the self-heating battery; (c) change in current and voltage of the cells during self-heating from −50 °C; (d) temperature evolutions of the Ni foils and cell surfaces during self-heating from −50 °C; (e) cell temperature evolution during self-heating from different ambient temperatures; (f) energy consumption in percentage of the cell electrical energy for self-heating from different temperatures.

cycles), which was less than half of that of FSI. At 75 °C, FSI had a cycle life of about 1900 h, while PF6 had a cycle life of less than 300 h. Even at an extremely high temperature of 90 °C when PF6 completely failed to operate, the FSI could be cycled for about 450 h. The superior cycle stability of FSI was mainly attributed to the high thermal stability of LiFSI, which suppressed electrolyte decomposition.[16] For all the capacity retention curves, they show a steady stage at first, and then at a point, the capacities deviate from the dashed line and drop faster.

A more straightforward figure plotting capacity loss vs square root of time is shown in Figure 1b. It is easy to see that the capacity loss curve was almost linear at first but then deviated from the linear part. The DCIR results in Figure 1c show that the deviation started almost simultaneously with the accelerated increase of resistance. The capacity decay in the first stage is mainly due to SEI growth, during which the electrolyte continues to react with the graphite and SEI thickens, and the capacity loss is almost linear with respect to $t^{1/2}$.[27−29] The continuous reaction of electrolyte with a graphite anode can cause loss of electrolyte and gas accumulation, and the accumulated SEI results in higher resistance that may cause lithium plating, all of which expedite capacity loss, and the capacity retention curve switches to the

second stage.[30] Overall, the cycle stability at high temperature was greatly improved by replacing LiPF$_6$ with LiFSI.

Robust low-temperature performance through rapid self-heating. Low temperature poses a big challenge for all batteries, due to the slower kinetics for mass transport and electrochemical reactions, which result in greatly increased resistance.[11] The DCIRs of FSI and PF6 at different temperatures were measured, as shown in Figure 2a. At room temperature (RT) of ∼22 °C, the DCIRs of FSI and PF6 are close to each other, i.e., 11.53 and 13.33 ohm·cm^2, respectively. As the temperature goes up, both cells show decreased DCIR owing to enhanced kinetics of electrochemical and transport processes. Conversely, when the temperature goes below room temperature, the DCIRs of both cells increase exponentially. The DCIR results are generally in accordance with the Arrhenius relationship. The DCIR of FSI is lower than that of PF6, which is consistent with the higher ionic conductivity of the LiFSI electrolyte reported in the literature, attributed to its higher dissociation and lower viscosity.[15] Due to the large DCIR, cells operating in subzero temperatures undergo severe drops in power and energy output, which limit the use in electric vehicles. The SHB can overcome this problem through fast and efficient internal heating using cell energy. Figure 2b shows a schematic of an SHB. Ni foil is embedded into the electrode stacks of a lithium-ion battery for
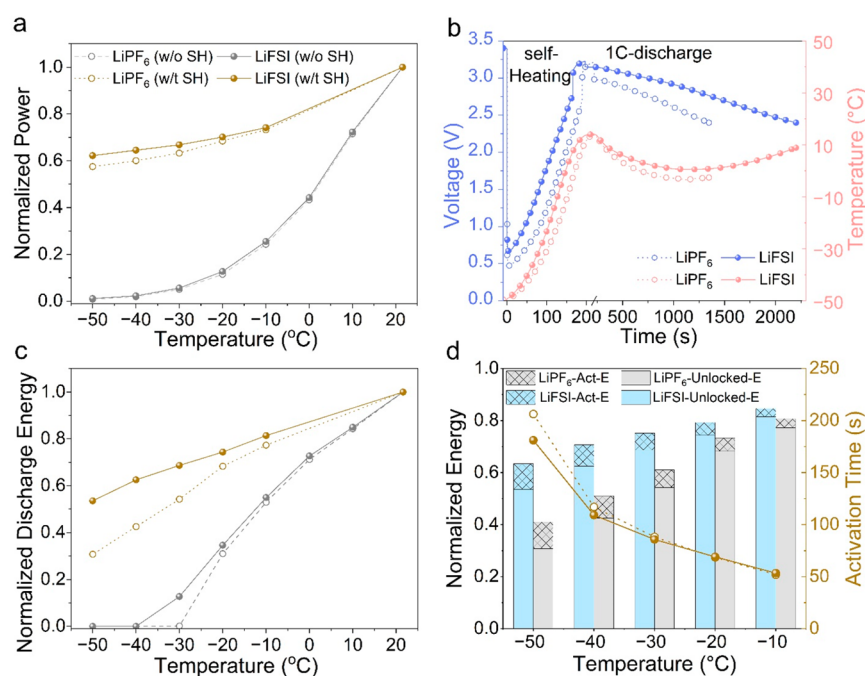
Figure 3. Power and energy boost with self-heating. (a) Battery power at different temperatures normalized to the room-temperature power with and without self-heating; **(b)** voltage and temperature profiles of the batteries during self-heating and discharge; **(c)** normalized discharge energy from different temperatures with and without self-heating; **(d)** activation energy, unlocked energy, and activation (heating + rest) time of cells at different ambient temperatures.

fast internal heating. One end of the Ni foil is welded into the negative tab, and the other is extended outside the battery as the activation (ACT) tab, and there is a switch wired between the positive and ACT tabs. With the switch OFF, the cell is used as a conventional, two-terminal cell. When the switch is ON, the current will flow from the positive electrode to and through the Ni foil and finally to the negative electrode. The heat generated in the Ni foil via Joule heating is rapidly transferred to the cell, quickly warming it up.

Figures 2c and S1 show the changes in current and voltage of the cells during the self-heating process, and Figure 2d shows the temperatures of the Ni foil and the cell outer surface during the self-heating process. As can be seen, when the switch was turned ON, current began to flow through the cell, and cell voltage dropped. With the flow of current, temperature rose, which in return increased the current due to decreased DCIR of the cell, and the cell was heated faster. When the cell temperature rose to a cutoff temperature of 10 °C, the switch was turned OFF, and there was no current. Within 15 s of rest after self-heating, the cell reached thermal equilibrium internally, and the temperature of the cell surface rose to about 15 °C. When comparing the heating currents at different ambient temperatures (T_{amb}), it is seen that the heating current decreased with decreasing T_{amb}. At −10 °C, the average heating currents of FSI and PF6 were close to each other (about 4.4 C); at −20 °C, the heating currents dropped slightly. At −30 °C, the average heating currents dropped to about 4 C, and the heating current of PF6 became noticeably smaller FSI. At −40 °C, the heating currents experienced a plunge, and the same thing happened at −50 °C.

The decreased heating current resulted in lower heating rates, as can be seen in Figure 2e. At −10, −20, and −30 °C, the heating rates of the two cells were close (about 0.66, 0.65, and 0.62 °C/s, respectively). When the ambient temperature

dropped to −40 °C, the heating rate of FSI (0.58 °C/s) became noticeably higher than that of PF6 (0.54 °C/s), and when the temperature dropped to −50 °C, the gap widened to 0.06 °C/s (i.e., 0.40 for FSI and 0.34 °C/s for PF6). The heating rates were generally consistent with the heating currents and DCIR. When it came to the energy consumption per degree of temperature rise of the cells during self-heating, it did not seem to vary with T_{amb}. For FSI, it consumed about 0.161% of the cell energy per °C, regardless of the ambient temperatures, following energy conservation.[3,19] For PF6, the energy consumption rate was about 0.167%·°C^{-1}. This indicates that the cells were well-insulated inside the box, and also there was very little heat loss due to the brief self-heating process. For FSI, it took only about 164 s and 10.44% of the cell energy to heat the cell from −50 to about 15 °C. This fast and energy-efficient self-heating technology makes it possible for cells to operate down to −50 °C even with commercially available electrolytes.

Remarkable power and energy at low temperatures. With the help of self-heating, significant boosts in the power and energy were achieved. Figure 3a shows the power of the battery normalized to its room-temperature power. As can be seen, without self-heating, for both cells, the delivered power decreased dramatically with decreasing temperature. When self-heating was applied prior to the delivery of power, the delivered power was greatly increased. For both cells, the boost in power with self-heating was about 20 times at −30 °C and about 200 times at −50 °C, owing to the greatly decreased DCIR after self-heating. The high power allows for the quick start-up of an EV when the ambient temperature is subzero. Besides power, boosts in energy output were also achieved by self-heating. Figure 3c shows the discharge energy of the cell normalized to its discharge energy at 22 °C at a discharge rate of 1C. Without self-heating, the discharge energy curves had a
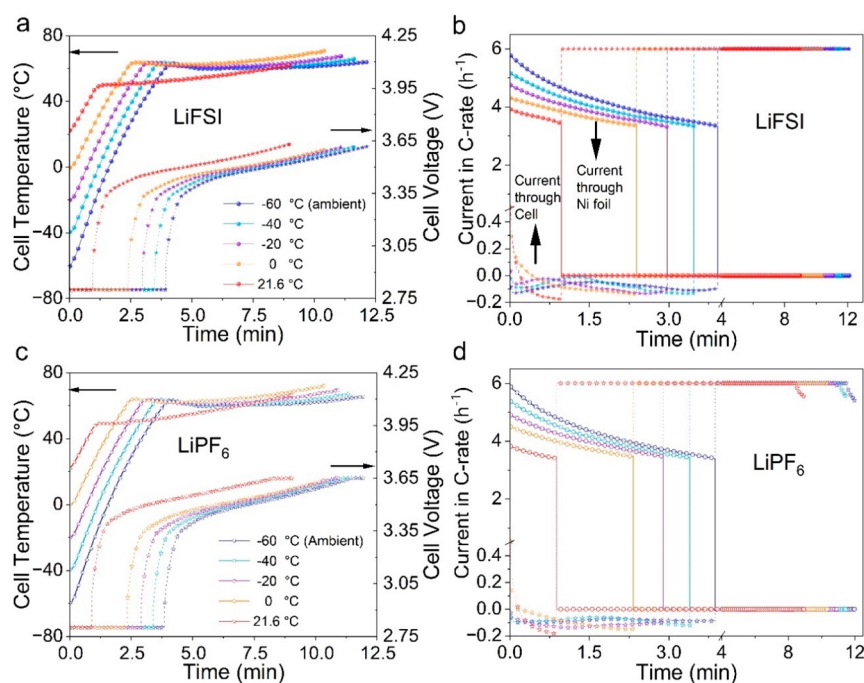
Figure 4. Fast preheating and 6C extreme fast-charging processes from different ambient temperatures: (a,c) Temperature and voltage profiles of FSI and PF6 cells, respectively; (b,d) currents through Ni foil for heating and through cell for charging for FSI and PF6, respectively, during the heating and 6C charging processes.

precipitous fall, with only about 30% at −20 °C for both cells. When the temperature dropped to −30 °C, PF6 had a sudden drop to almost 0, because the cell voltage hit the 2.4 V limit instantly upon discharging, and the same happened to FSI at −40 °C. The detailed discharge curves can be found in Figure S2. This is catastrophic for electric vehicles because the range would be greatly reduced, and they even fail to operate completely. Fortunately, when self-heating was introduced, the cells were first heated to a cutoff temperature of 10 °C using their own energy before discharging, and during the discharge process, the generated heat helped the cell to keep warm and continue to deliver energy until the voltage dropped to 2.4 V.

The detailed profiles of temperature and voltage during self-heating and 1C discharge can be found in Figures 3b and S3. After activation, the cell was discharged at 1C. In the discharge process, the cell temperature first decreased and then rose steadily owing to the continuous heat generation. When the ambient temperature was −10, −20, and −30 °C, the temperature profiles of FSI and PF6 were close, although PF6 finished discharging earlier due to the larger voltage drop. When the ambient temperature dropped to −40 and −50 °C, the discharge energy of PF6 was noticeably lower than FSI, probably due to exacerbated polarization effect.[31] As a result, although the delivered energy decreased with decreasing ambient temperature for both cells, FSI was able to deliver more energy compared with PF6, as shown in Figure 3c. For FSI, when self-heating was introduced, the cell was able to deliver 53.6% of the energy even when the ambient temperature was as low as −50 °C, and for PF6, it delivered only 30.7%. This is a great improvement for batteries that need to be exposed to extremely low temperatures, as self-heating is quick and efficient. Figure 4d summarizes the activation energy, unlocked energy, and activation time of the cells at different ambient temperatures. In general, as the ambient temperature decreases, it takes a longer time and more energy

for a cell to be activated, while the unlocked energy becomes smaller. But when comparing FSI and PF6, it is easy to see that FSI has noticeable better performance at lower temperatures.

6C fast charging from all temperatures. XFC is a major challenge facing lithium-ion batteries due to lithium plating that causes severe capacity decay and safety problems, especially when ambient temperature is low. For LFP/graphite cells, due to the low diffusion rate of Li ions in both the cathode and the anode, fast charging is especially difficult.[6] One solution to address this problem, as suggested in the literature, is to add low-viscosity solvents (such as methyl acetate) to increase the ionic conductivity of the electrolyte. Nonetheless, these low-viscosity solvents are highly volatile with very low boiling points (e.g., 57 °C for methyl acetate) and hence cannot withstand storage in elevated-temperature environments like hot summers. Thus, this solution is impractical. Previous studies have shown that lithium plating is more likely to happen at low temperatures and high SOCs.[32,33] When the cell is charging at a high temperature, due to the accelerated kinetics for the transport of Li⁺ in the electrolyte and diffusion of Li⁺ in electrodes, lithium plating can be effectively avoided.[34] We then use the fast internal heating technique to heat the cell to a high temperature (e.g., >60 °C) to increase the kinetics for mass transfer and electrochemical reactions while using standard electrolytes and charge the cell at high rates without lithium plating.

Figure 4 shows the change in voltage, temperature, and current in the cells during the preheating and charging process. All the cells were fully discharged at 22 °C and rested for about 10 h before testing. The open circuit voltage (OCV) of the cells were about 2.80 V. In the first step, the switch was turned on, and a constant voltage (CV) of 2.8 V was applied to the cell immediately. The voltage and temperature profiles are shown in Figure 4a,c. Since the applied voltage was close to OCV, in the heating step, most current went through the Ni
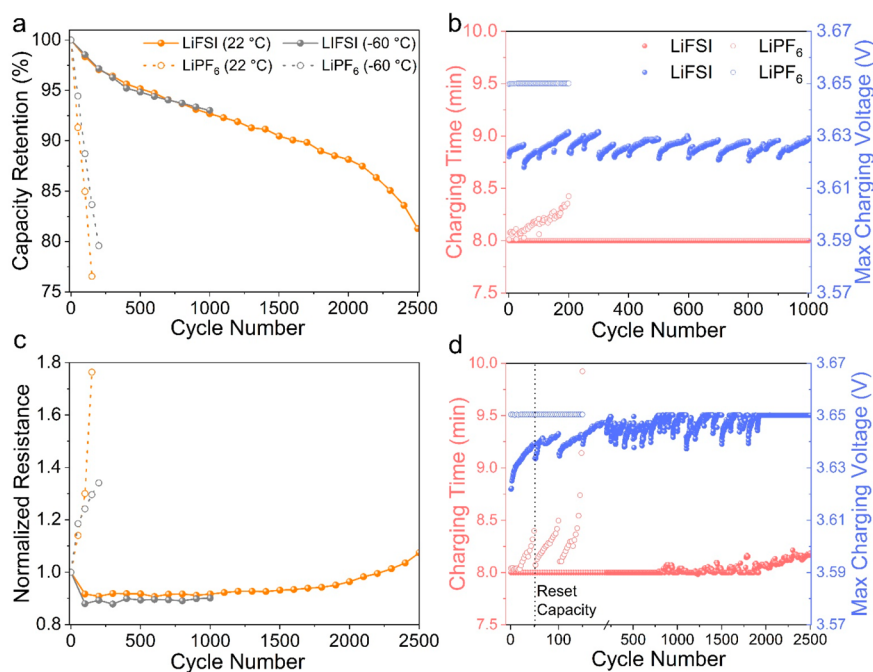
Figure 5. Cycle life of XFC cells. (a) Capacity retention of FSI and PF6 cells cycled at ambient temperatures of −60 and 22 °C; (b) charging time and max charging voltage of the cells at 22 °C; (c) change in direct current resistance during cycling; (d) change of charging time and max charging voltage of the cells at ambient temperature of −60 °C.

foil for heating, and very small current went through the cell, as can be seen from Figure 4b,d. Instead of being charged, the cell might be discharged slightly (equivalent to about 0.3% of cell capacity at −60 °C and 0.1% at 22 °C). This CV heating step ensured that the cells were not charged or deeply overdischarged during heating. The current through the Ni foil heated the cell rapidly. The heating current increased with decreasing T_{amb}, which was due to the decreased resistance of Ni foil at lower temperatures. When the cell temperature reached the cutoff temperature of 61 °C (except for T_{amb} of 22 °C, whose cutoff temperature was set to 46 °C, which will be explained later), the heating step was finished, and the switch was turned OFF. The internal heating was very quick and took about 0.96, 2.39, 2.97, 3.47, and 3.92 min at T_{amb} of 22, 0, −20, −40, and −60 °C, respectively. As shown in Figure S4 for preheating from −60 °C, the Ni foil reached the highest temperature of about 69.4 °C; this is 8.4 °C higher than the cell outer surface temperature. After heating is off, the Ni foil and cell outer surface reach an equilibrium temperature of about 63.5 °C in ~20 s.

After heating, a constant current corresponding to 6C was applied immediately, and since the switch was turned off, all currents must go through the cell for charging. During the XFC process, the cell produced a huge amount of heat, which helped to maintain and even increase the cell temperature, and thus, no additional heating was needed. The rise in temperature during charging increases with increasing ambient temperature due to less heat loss. At T_{amb} of 22 °C, if the cutoff temperature was set to 61 °C, the cell temperature would rise all the way to 78 °C during charging, which can be seen in Figure S5. Such high temperature may cause fast capacity decay, so the cutoff temperature was adjusted to 46 °C, and the temperature rose to only about 64 °C after charging. Figure 4a shows that FSI never hit the cutoff voltage of 3.65 V during charging to 80% SOC, and from T_{amb} of −60 to 0 °C, the

maximal voltage during charging decreased slightly, which was due to the higher temperature that decreased polarization. Meanwhile, for PF6, the cell kept hitting the cutoff voltage except for T_{amb} of 0 °C. This is also evident in Figure 4d, where the charging currents showed decreases at the CV step. From T_{amb} of −60 to 0 °C, the CV step decreased and even vanished due to the increased temperature during charging. The CV step increases the charging time. Although the CV step can be eliminated at higher temperatures, it has been shown in Figure 1 that high temperature causes severe capacity decay for PF6 and should be avoided. This causes a dilemma for PF6, which FSI avoided owing to the higher thermal stability. The total time for preheating and charging of the cells was less than 12 min, even when T_{amb} is as low as −60 °C, which made XFC possible and ubiquitous around the world.

Ultralong cycling life at 6C charging. The cycling stability of the XFC cells was then tested. Figure S6a,b presents the temperature and voltage profiles of FSI in three consecutive cycles tested at T_{amb} values of −60 and 22 °C, respectively. The heating and charging processes were similar to those presented in Figure 4, and after fast charging, the cell was rested for 10 min and then discharged at 1C to 2.4 V followed by a 1 min rest and C/3 discharge to 2.4 V and cooled to ambient temperature for the next cycle. This asymmetric thermal modulation (ATM) technique eliminates lithium plating during the charging step and at the same time minimizes the exposed time at high temperatures, as the degradation of cells is a function of the exposure time at high temperatures.[35,36] PF6 cells were also tested in the same ways for comparison. After every 50 cycles (for PF6) or 100 cycles (for FSI) of XFC, a reference performance test (RPT) was performed at 22 °C to characterize the state of health (SOH) and DCIR.

The measured capacities and resistances were normalized to the initial capacity and resistance, respectively, and are plotted

against cycle number in Figure 5a,c. For PF6, it experienced severe capacity decay after XFC, with over 20% capacity loss in less than 200 cycles, and noticeable increases in resistances were observed. It can also be seen from Figure 5b,d that PF6 always hit the cutoff voltage (3.65 V) in the charging step, and the charging time kept increasing during the XFC cycles before resetting after each RPT. More detailed information on the charging profile of the cells tested in 22 °C can be found in Figure S7. With continuous cycling, the average voltage during charging became higher, and the CV step became longer, which is consistent with the DCIR data. In the 150th cycle, the CV step became very long, and the charge current eventually dropped to below 1C, which markedly increases the charging time. Also, the cell had severe gas generation and swelling after cycling, which can be seen from Figure S8. In comparison, FSI has much better cycle stability at both 22 and −60 °C. At a T_{amb} of −60 °C, FSI experienced 1000 XFC cycles and still had a capacity retention of over 93.6%. The cell resistance was also much more stable and even decreased slightly after the first 100 cycles, which may be due to improved wetting of the electrolyte in the cell after exposure to high temperature. Looking at the voltage and charging time, the cell did not hit the CV step, and the charging time to 80% SOC is always 8 min. The max voltage during XFC increased with cycling, but once the capacity was reset, the max voltage went down again. For FSI operating at 22 °C, it had similar behavior, but it hit the CV step occasionally before resetting the capacity. This might be due to the higher average temperature in each cycle, which resulted in slightly faster SEI growth. Despite that, FSI tested at 22 °C finished 2500 XFC cycles and still had a capacity retention of over 80%, which is more than 10 times higher than PF6. Assuming that the range of a vehicle is 200 miles, then 80% SOC equals to 160 miles, and the XFC cycle life corresponds to a mileage of 400 000 or 33 years of life if an electric vehicle is charged once every 5 days, which exceeds the warranty coverage provided for internal combustion engine vehicles. Overall, FSI outperforms PF6 at both normal and extremely low ambient temperatures. The superior performance of FSI originates from the intrinsically more thermally stable LiFSI with higher conductivity and higher Li$^+$ transference number, which alleviates lithium plating and electrolyte decomposition that cause severe degradation of the battery.[37−39]

LFP has garnered increasing favor within the EV market due to its notable attributes, such as abundant raw materials, low cost, and high safety. However, its relatively lower energy density, slower charging rates, and limited temperature range have traditionally restricted its broader application, and concerns exist in industry that LFP cannot be fast-charged. In this study, the thermal modulatory cell design, combined with a commercially available electrolyte using single salt LiFSI, has substantially extended the operational temperature range of LFP to an impressive −50−90 °C, surpassing most real-world conditions. More remarkably, this advancement has enabled LFP to support 6C fast charging at all temperatures while maintaining an exceptional cycle life. The added thickness and weight due to Ni foils are 50 μm and 3.6 g, respectively, in our test cells of 11 mm in thickness and 218 g in weight, thus altering the volumetric and gravimetric energy densities only by 0.45 and 1.65%, respectively. Further reduction of the Ni foil thickness from 25 to 10 μm would shrink these numbers to 0.18 and 0.66%, respectively. Together, these results underscore the versatility of self-

heating technology, showcasing its potential for universal adaptation across batteries with different electrodes and electrolytes. The experimental data presented in this study hope to dispel doubts surrounding LFP, serving as an impetus for the widespread adoption of EVs.

■ ASSOCIATED CONTENT

ⓈＩ Supporting Information

The Supporting Information is available free of charge at https://pubs.acs.org/doi/10.1021/acsenergylett.3c02823.

> Experimental methods, resistances of Ni foils of the cells, current and voltage profiles during self-heating, discharge profiles without self-heating, voltage and temperature profiles during self-heating and 1C discharge, voltage and temperature profile during 6C charging, voltage and temperature profiles of three consecutive fast-charging cycles, current and voltage profiles of the cells at different cycles, optical images of the cells after XFC cycles, Li-plating detection (PDF)

■ AUTHOR INFORMATION

Corresponding Authors

Chao-Yang Wang − *Electrochemical Engine Center (ECEC) and Department of Mechanical Engineering, The Pennsylvania State University, University Park, Pennsylvania 16802, United States;* ⓞ orcid.org/0000-0003-0650-0025; Email: cxw31@psu.edu

Feifei Shi − *Department of Energy and Mineral Engineering and Materials Science and Engineering, The Pennsylvania State University, University Park, Pennsylvania 16802, United States;* ⓞ orcid.org/0000-0002-2598-1867; Email: feifeishi@psu.edu

Authors

Jie Liao − *Department of Materials Science and Engineering, The Pennsylvania State University, University Park, Pennsylvania 16802, United States;* ⓞ orcid.org/0009-0009-4716-660X

Ryan S. Longchamps − *EC Power, State College, Pennsylvania 16803, United States;* ⓞ orcid.org/0000-0002-8168-8032

Brian D. McCarthy − *EC Power, State College, Pennsylvania 16803, United States;* ⓞ orcid.org/0000-0002-2792-1681

Complete contact information is available at:
https://pubs.acs.org/10.1021/acsenergylett.3c02823

Notes

The authors declare no competing financial interest.

■ ACKNOWLEDGMENTS

■ REFERENCES

(1) Sathiyan, S. P.; Pratap, C. B.; Stonier, A. A.; Peter, G.; Sherine, A.; Praghash, K.; Ganji, V. Comprehensive Assessment of Electric Vehicle Development, Deployment, and Policy Initiatives to Reduce

GHG Emissions: Opportunities and Challenges. *IEEE Access* **2022**, *10*, 53614−53639.

(2) Cheng, X. B.; Liu, H.; Yuan, H.; Peng, H. J.; Tang, C.; Huang, J. Q.; Zhang, Q. A perspective on sustainable energy materials for lithium batteries. *SusMat* **2021**, *1* (1), 38−50.

(3) Yang, X-G.; Liu, T.; Wang, C-Y. Thermally modulated lithium iron phosphate batteries for mass-market electric vehicles. *Nature Energy* **2021**, *6* (2), 176−185.

(4) Li, J.; Ma, Z.-F. Past and Present of LiFePO4: From Fundamental Research to Industrial Applications. *Chem.* **2019**, *5* (1), 3−6.

(5) Murdock, B. E.; Toghill, K. E.; Tapia-Ruiz, N. A Perspective on the Sustainability of Cathode Materials used in Lithium-Ion Batteries. *Adv. Energy Mater.* **2021**, *11* (39), 2102028.

(6) Zhang, W.-J. Structure and performance of LiFePO4 cathode materials: A review. *J. Power Sources* **2011**, *196* (6), 2962−2970.

(7) Zhang, H.; Zou, Z.; Zhang, S.; Liu, J.; Zhong, S. A review of the Doping Modification of LiFePO4 as a Cathode Material for Lithium Ion Batteries. *Int. J. Electrochem. Sci.* **2020**, *15* (12), 12041−12067.

(8) Waldmann, T.; Wilka, M.; Kasper, M.; Fleischhammer, M.; Wohlfahrt-Mehrens, M. Temperature dependent ageing mechanisms in Lithium-ion batteries - A Post-Mortem study. *J. Power Sources* **2014**, *262*, 129−135.

(9) Huang, C. K.; Sakamoto, J. S.; Wolfenstine, J.; Surampudi, S. The Limits of Low-Temperature Performance of Li-Ion Cells. *J. Electrochem. Soc.* **2000**, *147* (8), 2893−2896.

(10) Xu, J.; Zhang, J.; Pollard, T. P.; Li, Q.; Tan, S.; Hou, S.; Wan, H.; Chen, F.; He, H.; Hu, E.; et al. Electrolyte design for Li-ion batteries under extreme operating conditions. *Nature* **2023**, *614* (7949), 694−700.

(11) Yang, Y.; Yang, W.; Yang, H.; Zhou, H. Electrolyte design principles for low-temperature lithium-ion batteries. *eScience* **2023**, *3* (6), 100170.

(12) Hou, J.; Yang, M.; Wang, D.; Zhang, J. Fundamentals and Challenges of Lithium Ion Batteries at Temperatures between −40 and 60 °C. *Adv. Energy Mater.* **2020**, *10* (18), 1904152.

(13) Logan, E. R.; Hebecker, H.; Eldesoky, A.; Luscombe, A.; Johnson, M. B.; Dahn, J. R. Performance and Degradation of LiFePO4/Graphite Cells: The Impact of Water Contamination and an Evaluation of Common Electrolyte Additives. *J. Electrochem. Soc.* **2020**, *167* (13), 130543.

(14) Chen, L.; Wu, H.; Ai, X.; Cao, Y.; Chen, Z. Toward wide-temperature electrolyte for lithium-ion batteries. *Battery Energy* **2022**, *1* (2), 20210006.

(15) Han, H.-B.; Zhou, S.-S.; Zhang, D.-J.; Feng, S.-W.; Li, L.-F.; Liu, K.; Feng, W.-F.; Nie, J.; Li, H.; Huang, X.-J. Lithium bis(fluorosulfonyl)imide (LiFSI) as conducting salt for nonaqueous liquid electrolytes for lithium-ion batteries: Physicochemical and electrochemical properties. *J. Power Sources* **2011**, *196* (7), 3623−3632.

(16) Logan, E. R.; Eldesoky, A.; Eastwood, E.; Hebecker, H.; Aiken, C. P.; Metzger, M.; Dahn, J. R. The Use of LiFSI and LiTFSI in LiFePO4/Graphite Pouch Cells to Improve High-Temperature Lifetime. *J. Electrochem. Soc.* **2022**, *169* (4), 040560.

(17) Wang, L.; Xu, S.; Wang, Z.; Yang, E.; Jiang, W.; Zhang, S.; Jian, X.; Hu, F. A nano fiber-gel composite electrolyte with high Li+ transference number for application in quasi-solid batteries. *eScience* **2023**, *3* (2), 100090.

(18) Wang, C.-Y.; Liu, T.; Yang, X.-G.; Ge, S.; Stanley, N. V.; Rountree, E. S.; Leng, Y.; McCarthy, B. D. Fast charging of energy-dense lithium-ion batteries. *Nature* **2022**, *611* (7936), 485−490.

(19) Wang, C.-Y.; Zhang, G.; Ge, S.; Xu, T.; Ji, Y.; Yang, X.-G.; Leng, Y. Lithium-ion battery structure that self-heats at low temperatures. *Nature* **2016**, *529* (7587), 515−518.

(20) Delacourt, C.; Poizot, P.; Levasseur, S.; Masquelier, C. Size effects on carbon-free LiFePO4 powders: The key to superior energy density. *Electrochem. Solid-State Lett.* **2006**, *9* (7), A352.

(21) Liang, J.; Gan, Y.; Yao, M.; Li, Y. Numerical analysis of capacity fading for a LiFePO4 battery under different current rates and ambient temperatures. *Int. J. Heat Mass Transfer* **2021**, *165*, 120615.

(22) Weiss, M.; Ruess, R.; Kasnatscheew, J.; Levartovsky, Y.; Levy, N. R.; Minnmann, P.; Stolz, L.; Waldmann, T.; Wohlfahrt-Mehrens, M.; Aurbach, D.; et al. Fast Charging of Lithium-Ion Batteries: A Review of Materials Aspects. *Adv. Energy Mater.* **2021**, *11* (33), 2101126.

(23) Xu, K.; Lam, Y.; Zhang, S. S.; Jow, T. R.; Curtis, T. B. Solvation sheath of Li+ in nonaqueous electrolytes and its implication of graphite/electrolyte interface chemistry. *J. Phys. Chem. C* **2007**, *111* (20), 7411−7421.

(24) Yang, X.-G.; Zhang, G.; Ge, S.; Wang, C.-Y. Fast charging of lithium-ion batteries at all temperatures. *Proc. Natl. Acad. Sci. U. S. A.* **2018**, *115* (28), 7266−7271.

(25) Xu, K. Nonaqueous liquid electrolytes for lithium-based rechargeable batteries. *Chem. Rev.* **2004**, *104* (10), 4303−4418.

(26) Guo, Z.; Chen, Z. High-temperature capacity fading mechanism for LiFePO4/graphite soft-packed cell without Fe dissolution. *J. Electroanal. Chem.* **2015**, *754*, 148−153.

(27) Zhu, W.; Zhou, P.; Ren, D.; Yang, M.; Rui, X.; Jin, C.; Shen, T.; Han, X.; Zheng, Y.; Lu, L.; Ouyang, M. A mechanistic calendar aging model of lithium-ion battery considering solid electrolyte interface growth. *International Journal of Energy Research* **2022**, *46* (11), 15521−15534.

(28) Lewerenz, M.; Münnix, J.; Schmalstieg, J.; Käbitz, S.; Knips, M.; Sauer, D. U. Systematic aging of commercial LiFePO 4 |Graphite cylindrical cells including a theory explaining rise of capacity during aging. *J. Power Sources* **2017**, *345*, 254−263.

(29) Attia, P. M.; Chueh, W. C.; Harris, S. J. Revisiting the t0.5 Dependence of SEI Growth. *J. Electrochem. Soc.* **2020**, *167* (9), 090535.

(30) Han, X.; Lu, L.; Zheng, Y.; Feng, X.; Li, Z.; Li, J.; Ouyang, M. A review on the key issues of the lithium ion battery degradation among the whole life cycle. *eTransportation* **2019**, *1*, 100005.

(31) Longchamps, R. S.; Yang, X.-G.; Ge, S.; Liu, T.; Wang, C.-Y. Transforming rate capability through self-heating of energy-dense and next-generation batteries. *J. Power Sources* **2021**, *510*, 230416.

(32) Qin, Y.; Zuo, P.; Chen, X.; Yuan, W.; Huang, R.; Yang, X.; Du, J.; Lu, L.; Han, X.; Ouyang, M. An ultra-fast charging strategy for lithium-ion battery at low temperature without lithium plating. *Journal of Energy Chemistry* **2022**, *72*, 442−452.

(33) Mei, W.; Zhang, L.; Sun, J.; Wang, Q. Experimental and numerical methods to investigate the overcharge caused lithium plating for lithium ion battery. *Energy storage materials* **2020**, *32*, 91−104.

(34) Yang, X.-G.; Liu, T.; Gao, Y.; Ge, S.; Leng, Y.; Wang, D.; Wang, C.-Y. Asymmetric Temperature Modulation for Extreme Fast Charging of Lithium-Ion Batteries. *Joule* **2019**, *3* (12), 3002−3019.

(35) Pinson, M. B.; Bazant, M. Z. Theory of SEI formation in rechargeable batteries: capacity fade, accelerated aging and lifetime prediction. *J. Electrochem. Soc.* **2013**, *160* (2), A243.

(36) Smith, A.; Burns, J. C.; Zhao, X.; Xiong, D.; Dahn, J. A high precision coulometry study of the SEI growth in Li/graphite cells. *J. Electrochem. Soc.* **2011**, *158* (5), A447.

(37) Du, Z.; Wood, D. L.; Belharouak, I. Enabling fast charging of high energy density Li-ion cells with high lithium ion transport electrolytes. *Electrochem. Commun.* **2019**, *103*, 109−113.

(38) Forestier, C.; Grugeon, S.; Davoisne, C.; Lecocq, A.; Marlair, G.; Armand, M.; Sannier, L.; Laruelle, S. Graphite electrode thermal behavior and solid electrolyte interphase investigations: Role of state-of-the-art binders, carbonate additives and lithium bis(fluorosulfonyl)-imide salt. *J. Power Sources* **2016**, *330*, 186−194.

(39) Yang, G.; Zhang, S.; Weng, S.; Li, X.; Wang, X.; Wang, Z.; Chen, L. Anionic Effect on Enhancing the Stability of a Solid Electrolyte Interphase Film for Lithium Deposition on Graphite. *Nano Lett.* **2021**, *21* (12), 5316−5323.